Coulomb-energy featured capture kinetics in graphene nanoribbon field-effect transistors

Ming-Pei Lu*
National Nano Device Laboratories, Hsinchu 300, Taiwan
(Received 26 April 2012; revised manuscript received 18 June 2012; published 23 July 2012)

Charges trapped in the gate dielectric and acting as long-range scatterers can have a significant effect on carrier transport in graphene-based nanodevices. In this study, we theoretically investigated the charge capture kinetics of short-distance channel-defect interactions in graphene nanoribbon nanodevices by employing the nonradiative multiphonon theory in conjunction with the Coulomb energy (ΔE). The peaks that emerged from the electron capture rate strongly correlated with the singularity characteristics of a one-dimensional (1D) density of states. Furthermore, we elaborate herein on how the value of ΔE plays a decisive role in determining the capture kinetics for the trapping of channel carriers in the interface dielectric defects in 1D nanodevices.

DOI: 10.1103/PhysRevB.86.045433 PACS number(s): 72.20.Jv, 73.22.−f, 85.35.−p, 63.20.kp

I. INTRODUCTION

Moore's law has driven the evolution of semiconductor manufacture through shrinking of the dimensions of field-effect transistors (FETs), thereby improving the switching performance of electronic circuits and lowering the costs of commercial chips.[1] As the dimensions of FETs have decreased to become comparable with the screening length, a new issue has arisen: significant repulsive Coulombic interactions between the channel carriers and the interface charged defects at short distance.[2–4] In particular, experimental observations of large-amplitude conductance switching, due to single charge capture, have appeared because of channel potential perturbation enhanced by the confinement effect in one-dimensional (1D) nanoFETs.[3,4]

Several 1D nanomaterials have been proposed to act as channels in nanoFETs to increase the carrier mobility and improve the gate electrostatic control of the channel potential relative to those of bulk Si MOSFETs.[5–8] Among those nanomaterials, graphene nanoribbons (GNRs) are particularly promising candidates for use in high-speed nanoelectronics and highly integrated nanochips,[7] potentially replacing Si in commercial nanoFETs,[8] because of their extremely high carrier mobilities[9] and tunable band gaps.[10,11] The semiconducting characteristics of GNRFETs featuring a GNR width of less than 10 nm have been demonstrated experimentally,[7] suggesting that continuous improvements in patterning technology will be necessary if narrow GNRs are to be fabricated to meet the future needs of the nanoelectronics industry. Furthermore, the effect of long-range charge scattering arising from the charged centers during carrier transport in graphene-based nanodevices has recently been highlighted.[12–14] As a result, it is highly likely that when the GNR width is scaled down to be comparable with the charge scattering length,[12] the charged dielectric defects will play a critical role in determining the physical characteristics of the GNRFETs. Nevertheless, relatively little is known about the capture kinetics behind the formation of interfacial charged dielectric defects in GNRFETs. Efforts dedicated to investigating the short-distance charge capture kinetics should shed light on the mechanism of long-range charged defect scattering and the physical origin of charge noise in GNRFETs.

In this study of short-distance channel-defect interactions in GNRFETs, we used correlated nonradiative multiphonon (NMP) theory in conjunction with the Coulomb energy (ΔE) to theoretically investigate the charge capture rate. To evaluate the values of ΔE, we developed a quantum capacitive circuit considering the effect of the fringing electrical field distributed spatially in the dielectric. The calculated short-distance charge capture rate for the channel subbands at room temperature revealed a significant correlation between the capture rate and the singularity characteristics of the 1D density of states (DOS).

It has been widely believed that charge capture through the NMP transition is responsible for the short-distance interactions between the channel carriers and the interfacial dielectric defects that are typically located within a few nanometers of the dielectric-channel interface.[15–17] Furthermore, by incorporating ΔE, regarded as the total work done by the voltage sources, into NMP theory, the experimental results for the short-distance charge capture in Si MOSFETs can be explained physically.[16,17] Therefore, in this study we investigated the short-range charge capture kinetics theoretically to obtain insight into the formation of long-range scattering centers in GNRFETs. Recently, several groups have demonstrated experimentally that graphene/GNR nanoFETs covered with a thin top-gate dielectric display improved switching characteristics,[18,19] suggesting that the incorporation of top-gate processes into nanoFET fabrication will be necessary to improve the performance of graphene-based nanoelectronics. For this reason, in this study we adopted top-gate GNRFETs with a thin SiO_2 gate dielectric as our device construction [Fig. 1(a)], with the source (S) and drain (D) metal electrodes directly contacting the ends of the GNR. The effect of doping on the electrical properties of GNRFET is beyond the scope of this paper; we are considering only the intrinsic characteristics of the GNR, implying that the chemical potential of the GNR (μ) will line up with the charge neutrality point (μ_0) at a top-gate voltage (V_G) of 0 V.

II. QUANTUM CAPACITIVE SYSTEM

From the point of view of electrical capacitance, two important capacitances are connected in series in the GNRFET: the gate capacitance C_G and the quantum capacitance C_Q. By considering capacitive coupling in the 1D nanoFET system and

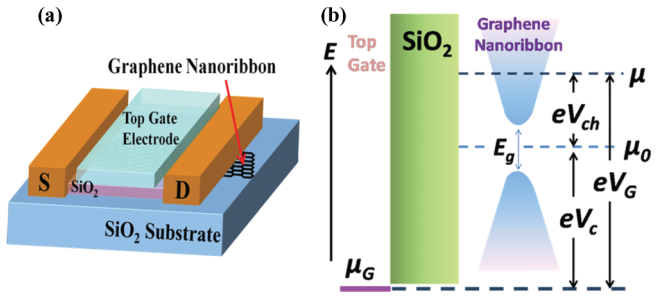

FIG. 1. (Color online) (a) Device structure of the GNRFET featuring a thin SiO_2 gate dielectric on the GNR. (b) Band structure of the 1D electronic system for the GNRFET; μ_G, $V_{\rm ch}$, and V_c are the chemical potential of the top-gate metal electrode, the surface potential shift with respect to the charge neutrality point, and the energy level of the charge neutrality point μ_0, respectively, when V_G is applied to the gate electrode.

assuming the presence of smooth electrostatic confinement in the GNR, the potential correlation between the value of V_G and the chemical potential μ can be written as[20,21]

$$eV_G = \mu - \mu_G = eV_c + eV_{\rm ch} = e^2 n_{\rm 1D}/C_G + (\mu - \mu_0), \tag{1}$$

where μ_G, $V_{\rm ch}$, and V_c are the chemical potential of the top-gate metal electrode, the surface potential shift with respect to the charge neutrality point, and the potential of the charge neutrality point μ_0, respectively, when the top-gate voltage equals V_G; $n_{\rm 1D}$ and e are the electron density of the GNR and the elementary charge, respectively. Figure 1(b) illustrates the band structure of the top-gate GNRFET having a GNR band gap of E_g.

Investigations of the cutting of armchair-edged GNR (a-GNR) from two-dimensional (2D) single-layer graphene[22] have recently attracted much attention because its band gap is tunable depending on the a-GNR width, the crystallographic orientation, and the edge effect.[10,11] In this 1D quantum system, the DOS for the ith subband in a-GNR can be written as

$$D_i(E) = \frac{g}{\pi\sqrt{3}ta}\frac{|E|}{\sqrt{E^2 - E_i^2}} \times U(|E| - |E_i|), \tag{2}$$

where g is the degenerate factor, t is the first-neighbor hopping integral, and a is the graphene lattice constant; i and U are an integer ($\pm1, \pm2, \ldots$) and the unit step function, respectively; E_n is the subband energy defined by a band structure model using a tight-binding calculation with considerations of the effects of C-C bond-length contraction at the GNR edge and $K-K'$ orbital splitting.[23] The band gap E_g for a-GNR with a width W can be expressed as $E_g = 2|\alpha|\pi\hbar\upsilon_f/W$, where υ_f is the Fermi velocity ($\sim 1 \times 10^6$ m/s).[23] Thus, values of E_g of 0.454 and 0.221 eV correspond to values of N_a of 21 and 42, respectively, where N_a is the number of dimer lines across the a-GNR width; the corresponding widths of a-GNR are approximately 2.4 and 5.0 nm, respectively. Figure 2(a) displays the calculated quantum capacitance (C_Q) normalized to the GNR width, defined as $C_Q = \frac{e}{W}\frac{\partial n_{\rm 1D}}{\partial V_{\rm ch}}$, for values of N_a of 21 and 42. Because of the abundance of the DOS at the bottom of the 1D subband, peaks appeared in the

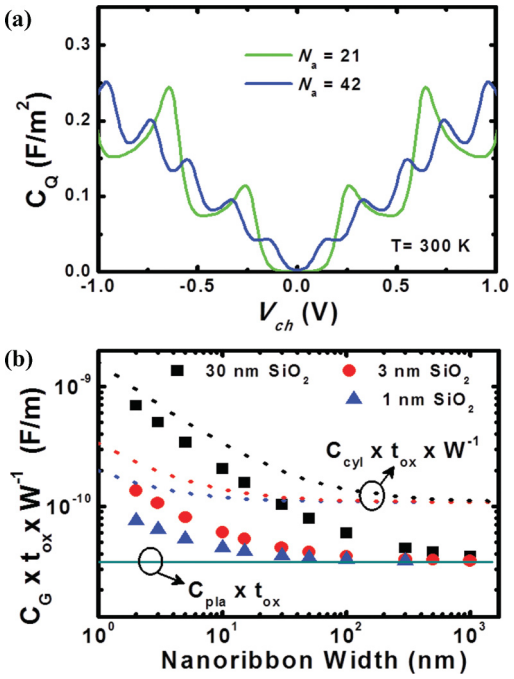

FIG. 2. (Color online) (a) Calculated values of C_Q normalized by the GNR width W plotted with respect to the surface potential shift $V_{\rm ch}$, for values of N_a of 21 and 42, at room temperature. (b) Values of C_G normalized by the GNR width W multiplied by the gate dielectric thickness $t_{\rm ox}$, plotted with respect to the GNR width W for values of $t_{\rm ox}$ of 1 nm (blue triangles), 3 nm (red dots), and 30 nm (black squares). The planar capacitance $C_{\rm pla}$ (solid lines) and the cylindrical capacitance $C_{\rm cyl}$ (blue, red, and black dotted lines for values of $t_{\rm ox}$ of 1, 3, and 30 nm, respectively) are also plotted for comparison.

values of C_Q of the GNR when μ approached each subband energy level. Furthermore, to obtain the quantum capacitive circuit for the evaluation of ΔE, we performed simulations using the finite-element method (FEM) to calculate the gate capacitance C_G including the effect of the fringing electrical field distributed spatially in SiO_2 dielectrics in the direction of the GNR's width. To highlight the effect of the fringing electrical field on the value of C_G, Fig. 2(b) displays the calculated values of C_G normalized to the GNR width W multiplied by the dielectric thickness $t_{\rm ox}$. The simulated values of C_G for values of $t_{\rm ox}$ of 1 nm (blue triangles), 3 nm (red dots), and 30 nm (black squares) are plotted with respect to GNR widths ranging from 1000 to 2 nm. Moreover, the planar gate capacitances are also displayed as a solid line in Fig. 2(a), determined using the expression $C_{\rm pla} = \kappa\varepsilon_0/t_{\rm ox}$, where κ is the relative dielectric constant. Through comparisons between the calculated values of C_G and the planar capacitance $C_{\rm pla}$, we conclude that the fringing electrical field effect can be ignored in the top-gate nanoFETs only when the value of $W/t_{\rm ox}$ is much greater than 10. On the other hand, when W is much less than $t_{\rm ox}$, the value of C_G will be approximately limited by the cylindrical-like capacitance [dotted lines, Fig. 2(b)], determined using the expression $C_{\rm cyl} \sim 2\pi\kappa\varepsilon_0/\ln(1 + 2t_{\rm ox}/W)$. This discussion suggests that considering the effect of the fringing electrical field on the gate capacitance C_G is necessary for GNRFETs featuring a narrow GNR.

III. CALCULATION OF CHARGE CAPTURE KINETICS

A. Coulomb energy

From the physical viewpoint, the degree of wave function overlapping corresponding to the interactions between the dielectric defect and the channel carriers will decrease when moving the defect away from the channel-dielectric interface and placing it deeper within the dielectric bulk. Furthermore, recent reports have revealed that the role played by interfacial charged defects is more decisive than that of dielectric bulk defects in terms of causing long-range Coulomb scattering and electrostatic doping.[24,25] For these reasons, we wished to pay attention to the short-distance channel-defect interactions associated with the interfacial dielectric defects. Note that small drain-to-source voltages are typically applied to ultrahigh-mobility nanoFETs to reduce power consumption and avoid self-heating effects, strongly suggesting that the voltage potentials of the S and D electrodes can be considered as the connections to the ground; therefore, it is reasonable to neglect the contributions of the S and D voltage potentials to the modulation of channel surface potential in GNR, as well as the value of ΔE. To restrict our attention in this report to the capture kinetics for electron carriers, we have excluded the hole-dominated region in the GNRFETs ($V_G < 0$ V). Thus, by considering the neutral dielectric defect, which can be regarded as an atomic point, located at the interface between the GNR and the SiO_2 gate dielectric, the value of ΔE accounting for the total work done by the voltage sources can be obtained:[17,26]

$$\Delta E \approx Q_G\, V_G = \frac{C_G}{C_G + C_Q}\, V_G, \tag{3}$$

where Q_G possessing opposite polarity to the trapped charge is the image charge at the top-gate electrode side. In a practical sense, when an electron is inserted into the neutral interface defect, an amount of positive charge Q_G will be simultaneously transferred from the ground through the gate voltage source to the top-gate electrode (inset to Fig. 3). Figure 3 displays a semilogarithmic plot of the calculated values of ΔE with respect to the electron density per unit area, for values of N_a of 21 and 42. We attribute the larger magnitude of ΔE at a value of t_{ox} of 1 nm to the larger value of Q_G as the result of the higher value of C_G, relative to that of the 30-nm-thick system. Moreover, the ripples in the plot of ΔE may be due to the peaks featured in the plot of C_Q [Fig. 2(a)], originating fundamentally from the singularity feature of the 1D DOS. Notably, in contrast to the decreasing values of ΔE upon increasing the carrier density of bulk Si MOSFETs from a few hundreds of milli–electron volts ($\sim$ 250 meV) to a few tens of milli–electron volts in the region of high carrier density,[17,26] the values of ΔE for a-GNRFETs featuring 1- and 30-nm SiO_2 dielectrics displayed increasing trends accompanied by apparent ripple characteristics, resulting in a value of ΔE of approximately 400 meV at a high electron density of approximately 10^{17} m^{-2}.

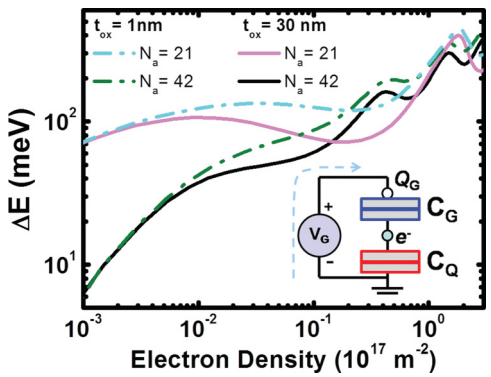

FIG. 3. (Color online) Calculated Coulomb energies for the a-GNRFETs with values of N_a of 21 and 42, plotted with respect to the electron density (m^{-2}) for values of t_{ox} of 1 and 30 nm. Inset: Representative illustration of the charge transfer process for the image charge Q_G.

B. Nonradiative multiphonon transition

Previous studies[16,17] have revealed that the capture kinetics for the short-distance charge-defect interaction can be described physically using NMP theory in conjunction with values of ΔE. Using this approach, the capture rate ($P_{c,i}$) for the trapping of a channel electron from the ith subband of the GNR to the interface defect through a short-distance NMP transition can be obtained using the formula

$$P_{c,i} = \bar{P}_{ph,i}\, \frac{n_{1D,i}}{W}\, e^{-\Delta E/(k_B T)}, \tag{4}$$

where $\bar{P}_{ph,i}$, $n_{1D,i}$, and W are the mean capture rate, the electron density per unit length for the ith subband of the GNR, and the GNR width, respectively. By taking into account the effect of the spatial carrier distribution in the direction of the GNR width, the average electron density per unit area ($n_{1D,i}/W$) for each subband will be incorporated into Eq. (4). Based on the theory of lattice relaxation for charged dielectric defects, two significant factors determine the strength of electron-phonon coupling in NMP theory: Huang-Rhys factors S and the phonon energy $\hbar\omega$.[16,17,27] A large lattice relaxation energy ($S\hbar\omega$) of 1–2 eV for SiO_2 dielectric defects is typically extracted from the experimental data for short-distance charge capture.[16,17] Therefore, in this study it was reasonable to apply a situation of strong lattice coupling. Using the Born-Oppenheimer approximation, the capture rate for an electron having an energy E from the ith subband with the strong lattice coupling can be written as[27,28]

$$P_{\mathrm{ph},i}(E) = \sigma_{0,i}\, \upsilon_f \exp\left[\frac{E_T + E}{2k_B T} - S \coth\left(\frac{\hbar\omega}{2k_B T}\right)\right] \times I_{(E_T+E)/\hbar\omega}\left(\frac{S}{\sinh(\hbar\omega/2k_B T)}\right), \tag{5}$$

where E_T is the defect energy, $\sigma_{0,i}$ is a constant factor corresponding to the wave function overlapping between the interface defect state and the channel carrier, and $I_{(E_T+E)/\hbar\omega}$ is the modified Bessel function. According to Eq. (5), $P_{\mathrm{ph},i}$ is a function of the electron energy E. To average the effect of the value of E on the NMP capture rate, the mean value of $P_{\mathrm{ph},i}$ can be defined as

$$\bar{P}_{\mathrm{ph},i} = \int P_{\mathrm{ph},i}(E) D_i(E) f(E) dE \Big/ \int D_i(E) f(E) dE, \tag{6}$$

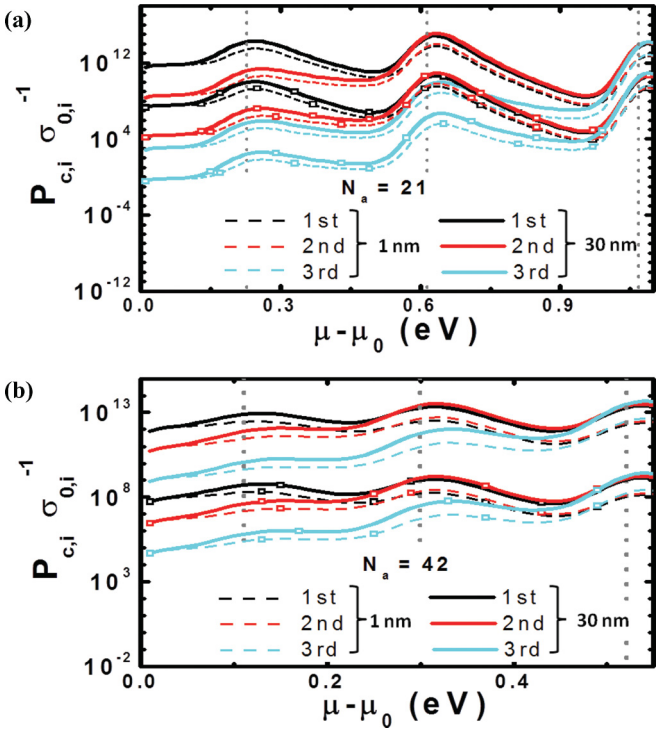

FIG. 4. (Color online) Theoretical values of $P_{c,i}/\sigma_{0,i}$ plotted with respect to the chemical potential shift $\mu - \mu_0$ for the first, second, and third channel subbands of the a-GNR at values of N_a of (a) 21 and (b) 42. The theoretically calculated results for Huang-Rhys factors (S) of 50 and 100 are denoted as lines drawn without and with empty squares, respectively. The vertical dotted lines correspond to each subband energy level, with the $K-K'$ orbital splitting effect included.

where $D_i(E)$ is the 1D DOS for the ith subband of the GNR and $f(E)$ is the Fermi-Dirac distribution function.

By considering an interfacial dielectric defect having a typical value of E_T of 3.2 eV relative to the conduction band of a SiO_2 dielectric[15,17,26] and a phonon energy $\hbar\omega$ of 20 meV for SiO_2 dielectric defect,[16,29] we used Eq. (4) to calculate the NMP capture rate for each subband. To investigate the impact of the values of the S on the charge capture kinetics, Fig. 4 displays the calculated results for values of S of 50 and 100 corresponding to lattice relaxation energy of 1 and 2 eV, respectively. Because of the higher electron occupation probabilities for the lower subbands, only the capture rates for the lowest three subbands are considered here. At present, we lack sufficient information to theoretically evaluate the constant factor $\sigma_{0,i}$ for each channel subband. Therefore, we divided the calculated value of $P_{c,i}$ by the constant factor $\sigma_{0,i}$ to investigate the short-distance capture kinetics [Figs. 4(a) and 4(b)]. The vertical dotted lines corresponding to each energy level of the channel subbands for values of N_a of 21 and 42 are plotted in Figs. 4(a) and 4(b), respectively. We find that the defect with a lower value of S had the higher charge capture rate. More importantly, the plots of $P_{c,i}/\sigma_{0,i}$ for each subband feature several consecutive peaks commonly located at specific energy levels. By comparing the relative position between the peaks and the subband energy levels, we conclude that the peaks in the plots of $P_{c,i}/\sigma_{0,i}$ appear only when the value of μ is nearly aligned with each subband energy level. As a result, the decrease in the value of ΔE originating from the peaks in the plot of C_Q will greatly enhance the short-distance capture rate. Notably, the total capture rate, summed statistically from the contribution of each subband by using the occupation weighting, would reveal consecutive peak features similar to the calculated results illustrated in Fig. 4. More extensively, if the value of μ were to be manipulated intentionally at the position of each valley in the capture rate, the lower NMP capture rate for short-distance channel-defect interactions would probably diminish the long-range charged defect scattering in GNRFETs.

IV. DISCUSSION AND CONCLUSIONS

Rather than employing the classical Shockley-Read-Hall theory, which has been used to describe a capture process displaying a linearly proportional relationship between the charge concentration and the capture rate,[30] the NMP transition considering the lattice relaxation process has been adopted widely over the past few decades to explore the thermal activation capture arising from short-distance channel-defect interactions.[15–17] Furthermore, values of ΔE have been incorporated into the NMP theory to physically correlate the capture kinetics in Si MOSFETs.[16,17] Importantly, the thermal activation barrier (E_B) for the NMP capture and the values of ΔE for the interface dielectric defects have been reported in the ranges 100–520 and 50–250 meV, respectively.[16,17,26] Accordingly, due to ΔE possessing the decreasing values upon increasing the carrier density, it is highly likely that the E_B would mainly govern the short-distance charge capture rate in the region of high carrier density of bulk Si MOSFETs. Furthermore, effective barriers of approximately 100 meV have been reported for channel-defect interactions in graphene/dielectric systems,[24,25] implying that the much larger value of ΔE, calculated to be approximately 400 meV, at a high electron density in the a-GNRFETs would play a decisive role in the short-distance capture kinetics of 1D nanoFETs. To date, only a few experimental results have appeared regarding the use of the transient charging measurement to extract the time constant of charge trapping in graphene nanodevices.[31,32] Through comparisons with those experimental results, it appears that the charge capture time constants measured using the higher value of V_G (~70 V)[31] were much longer than those for the other case using a smaller value of V_G (~30 V).[32] We suspect that a large value of ΔE that arises from a higher value of V_G in nanodevices may modulate the charge capture kinetics, resulting in the long charge-capture time constants. Further investigations will be needed to examine the effects of the value of ΔE on the charge capture kinetics in nanodevices.

In summary, we have theoretically investigated the capture kinetics of the NMP transition responsible for short-distance channel-defect interactions in top-gate a-GNRFETs at room temperature to elucidate the significant effect of the value of ΔE on the charge capture rate in 1D nanoFETs. The consecutive peaks in the calculated capture rate highlight the significant role of the value of ΔE in the short-distance charge capture of GNRFETs. This study not only paves the way toward an elaboration of the capture kinetics for

short-distance channel-defect interactions in 1D nanoFETs but also suggests that such systems can be applied in the fields of 1D nanoelectronics, single-charge nanomemories,[33,34] and single-electron nanodevices.[35,36]

ACKNOWLEDGMENTS

We thank the National Science Council of Taiwan (NSC100-2221-E-492-006 and NSC101-2221-E-492-001) for financial support.

*mingpei.lu@gmail.com

[1]S. E. Thompson and S. Parthasarathy, Mater. Today **9**, 20 (2006).
[2]M. J. Chen and M. P. Lu, Appl. Phys. Lett. **81**, 3488 (2002).
[3]J. Salfi, I. Savelyev, M. Blumin, S. Nair, and H. Ruda, Nat. Nanotechnol. **5**, 737 (2010).
[4]N. Clément, K. Nishiguchi, A. Fujiwara, and D. Vuillaume, Nat. Commun. **1**, 92 (2010).
[5]Y. Cui and C. M. Lieber, Science **291**, 851 (2001).
[6]J. Xiang, W. Lu, Y. Hu, Y. Wu, H. Yan, and C. M. Lieber, Nature (London) **441**, 489 (2006).
[7]X. Wang, Y. Ouyang, X. Li, H. Wang, J. Guo, and H. Dai, Phys. Rev. Lett. **100**, 206803 (2008).
[8]F. Schwierz, Nat. Nanotechnol. **5**, 487 (2010).
[9]L. Liao, J. Bai, Y. Qu, Y. Lin, Y. Li, Y. Huang, and X. Duan, Proc. Natl. Acad. Sci. USA **107**, 6711 (2010).
[10]Y. W. Son, M. L. Cohen, and S. G. Louie, Phys. Rev. Lett. **97**, 216803 (2006).
[11]M. Y. Han, B. Özyilmaz, Y. Zhang, and P. Kim, Phys. Rev. Lett. **98**, 206805 (2007).
[12]J. Martin, N. Akerman, G. Ulbricht, T. Lohmann, J. Smet, K. Von Klitzing, and A. Yacoby, Nat. Phys. **4**, 144 (2007).
[13]S. Adam, E. Hwang, V. Galitski, and S. Das Sarma, Proc. Natl. Acad. Sci. USA **104**, 18392 (2007).
[14]E. H. Hwang, S. Adam, and S. Das Sarma, Phys. Rev. Lett. **98**, 186806 (2007).
[15]M. Kirton and M. Uren, Adv. Phys. **38**, 367 (1989).
[16]A. Palma, A. Godoy, J. A. Jimenez-Tejada, J. E. Carceller, and J. A. Lopez-Villanueva, Phys. Rev. B **56**, 9565 (1997).
[17]M. P. Lu and M. J. Chen, Phys. Rev. B **72**, 235417 (2005).
[18]L. Liao, J. Bai, R. Cheng, Y. C. Lin, S. Jiang, Y. Huang, and X. Duan, Nano Lett. **10**, 1917 (2010).
[19]F. Xia, D. B. Farmer, Y. Lin, and P. Avouris, Nano Lett. **10**, 715 (2010).
[20]M. P. Lu, C. Y. Hsiao, P. Y. Lo, J. H. Wei, Y. S. Yang, and M. J. Chen, Appl. Phys. Lett. **88**, 053114 (2006).
[21]A. A. Shylau, J. W. Kłos, and I. V. Zozoulenko, Phys. Rev. B **80**, 205402 (2009).
[22]K. Novoselov, A. Geim, S. Morozov, D. Jiang, M. I. K. I. V. Grigorieva, S. Dubonos, and A. Firsov, Nature (London) **438**, 197 (2005).
[23]Y. M. Lin, V. Perebeinos, Z. Chen, and P. Avouris, Phys. Rev. B **78**, 161409 (2008).
[24]D. B. Farmer, V. Perebeinos, Y. M. Lin, C. Dimitrakopoulos, and P. Avouris, Phys. Rev. B **84**, 205417 (2011).
[25]H. Y. Chiu, V. Perebeinos, Y. M. Lin, and P. Avouris, Nano Lett. **10**, 4634 (2010).
[26]M. Schulz, J. Appl. Phys. **74**, 2649 (1993).
[27]M. Isler and D. Liebig, Phys. Rev. B **61**, 7483 (2000).
[28]C. Henry and D. V. Lang, Phys. Rev. B **15**, 989 (1977).
[29]W. B. Fowler, J. K. Rudra, M. E. Zvanut, and F. J. Feigl, Phys. Rev. B **41**, 8313 (1990).
[30]S. M. Sze, *Physics of Semiconductor Devices* (Wiley, New York, 1981).
[31]P. Joshi, H. Romero, A. Neal, V. Toutam, and S. Tadigadapa, J. Phys.: Condens. Matter **22**, 334214 (2010).
[32]Y. G. Lee, C. G. Kang, U. J. Jung, J. J. Kim, H. J. Hwang, H. J. Chung, S. Seo, R. Choi, and B. H. Lee, Appl. Phys. Lett. **98**, 183508 (2011).
[33]M. Fuhrer, B. Kim, T. Dürkop, and T. Brintlinger, Nano Lett. **2**, 755 (2002).
[34]C. Thelander, H. A. Nilsson, L. E. Jensen, and L. Samuelson, Nano Lett. **5**, 635 (2005).
[35]S. Kubatkin, A. Danilov, M. Hjort, J. Cornil, J. L. Brédas, N. Stuhr-Hansen, P. Hedegard, and T. Bjornholm, Nature (London) **425**, 698 (2003).
[36]C. Stampfer, E. Schurtenberger, F. Molitor, J. Guttinger, T. Ihn, and K. Ensslin, Nano Lett. **8**, 2378 (2008).